The University Of Sheffield.

This is a repository copy of *Simulation study of thermally initiated rail defects*.

White Rose Research Online URL for this paper:
http://eprints.whiterose.ac.uk/86303/

Version: Accepted Version

Article:
Fletcher, D., Scott, D. and Cardwell, B.J. (2012) Simulation study of thermally initiated rail defects. Proceedings of the Institution of Mechanical Engineers. Part F: Journal of Rail and Rapid Transit, 228 (2). pp. 113-127. ISSN 0954-4097

https://doi.org/10.1177/0954409712465697

Reuse
Unless indicated otherwise, fulltext items are protected by copyright with all rights reserved. The copyright exception in section 29 of the Copyright, Designs and Patents Act 1988 allows the making of a single copy solely for the purpose of non-commercial research or private study within the limits of fair dealing. The publisher or other rights-holder may allow further reproduction and re-use of this version - refer to the White Rose Research Online record for this item. Where records identify the publisher as the copyright holder, users can verify any specific terms of use on the publisher's website.

Takedown
If you consider content in White Rose Research Online to be in breach of UK law, please notify us by emailing eprints@whiterose.ac.uk including the URL of the record and the reason for the withdrawal request.

White Rose university consortium
Universities of Leeds, Sheffield & York

eprints@whiterose.ac.uk
https://eprints.whiterose.ac.uk/

Simulation Study of Thermally Initiated Rail Defects

D. Scott[1], D.I. Fletcher[2] and B.J. Cardwell[3]

[1] *Strategy & Service Development Directorate, London Underground, 55 Broadway, London. SW1H OBD*

[2] *MERail Railway Research Group, Department of Mechanical Engineering, University of Sheffield, Mappin Street, Sheffield. S1 3JD*

[3] *Independent Railway Simulation Expert for London Underground*

Abstract: Ultrasonically detected 'squat type' rail defects are becoming increasingly common on railways throughout the world. On the London Underground these defects are found on three lines. Focussing on the difference between these lines and others on the LU Network has identified vehicles with modern AC traction characteristics as a common theme found only on problem lines.

Metallurgical analysis of the defects found that the mechanisms for generation and growth are not consistent with conventional rolling contact fatigue, with evidence of significant thermal input. The defects are only found on open sections. The most susceptible areas to the defects are those where low speed running is more common.

A mathematical model of the traction package examined the forces and thermal input generated at the wheel-rail interface with modern wheel-spin control systems under wheel slip and adhesion recovery conditions. The outputs have been analysed to assess whether sufficient forces and temperatures are generated to explain the observed rail damage. The results suggest that under certain circumstances wheel-spin recovery generates sufficient rail surface energy for martensitic transformation. Additional modelling suggests that thermal input from wheel-spin aids crack propagation and that regions of slightly degraded (wet as opposed to leaf or oil contaminated) rail adhesion are sufficient to initiate these flaws.

Keywords: squat, ultrasonic defect, thermal defect, wheel-spin, AC traction, creep control, spin recovery, wheel-rail interface, martensite

1. INTRODUCTION

A gradual and systematic increase in rail defects has been recorded on certain London Underground (LU) lines over a period of years. Whilst superficially similar to other rolling contact fatigue "squat" failures these defects have unique features, most notably they are associated with a thermal input to the rail surface, as evidenced by metallurgical analysis of failed track sections. A multi-disciplinary investigation was initiated to understand both the physical characteristics and causes of this new phenomenon. This paper primarily concerns the contribution made by cross-discipline simulation of rail vehicle and track to produce a robust appreciation of the processes leading to the formation of thermally induced squat type track defects.

1.1 Background

Metallurgical investigation and the overall defect patterns strongly suggest the mechanism generating squat type defects on affected LU lines is different to standard rolling contact fatigue squats, which usually result from repetitive mechanical action, plastic flow and propagation assisted by fluid entry into the cracks [1]. More than 900 squat type defects, predominantly thermally initiated, were discovered on the Central Line in 2010/11. These were distributed widely throughout surface (above ground) sections; however, in proximity to platforms areas the number of defects was statistically insignificant. There was no apparent correlation with the acceleration or braking characteristic at stations. In surface sections some areas were affected significantly more than others, showing correlation with high traffic congestion points.

The other routes having defect incidents are Northern and Jubilee Lines. Analysis of Northern Line defects showed evidence of thermal damage, quite distinct from standard rail squat defects. Again, these incidents only occurred on surface track sections that could be exposed to weather elements, with evidence of predominance in low speed sections. There was no defect location statistical bias found between left and right rail.

The rolling stock on LU usually remains on a specific line, so the possibility of a link between the generation of defects and the rolling stock type was examined. It was found that the new squat type defect is restricted to modern AC and DC separately excited motor fleet lines, not the traditional DC series motor rolling stock used on other lines. There was no observable indication why modern traction equipment should be more vulnerable, but initial consideration focused around the steeper slope of the tractive effort (TE) - speed characteristic of these motor systems. These drive systems have been introduced on many modern metro and underground fleets to give better initial acceleration, thereby increasing system capacity.

1.2 Rolling Stock and Track Characteristics

Assessment of distribution led the squat rail defects to be assessed as a traction originated event. It is necessary to understand the mechanical and physical behaviour of both the wheel-rail interface (WRI) and the traction system in this instance to establish the root cause. This is extremely difficult to achieve via track measurements. Therefore, with a base of traction modelling work conducted during commissioning of 1992 Tube Stock (92TS), which operates on Central Line, it was proposed to develop a new rolling stock / track model as an investigative tool.

The modelling requirements are discussed in Section 3.1, however, the characteristics of the rolling stock plays an important role. 92TS employs separately excited DC traction motors with two armatures in series under chopper control. The total of four armature strings per two-cars have a common field current provided by the connection of all eight fields in series supplied by a single field chopper. The traction characteristics for motoring are depicted in Figure 1, showing high TE at low speed to achieve good initial acceleration. This is vital for good vehicle headways and passenger throughput on any urban or metro rail system. The rolling stock normally operates by Automatic Train Operation (ATO), which produces cyclic motor-brake behaviour in traffic or when running against speed limits. An example is shown in Figure 2.

The process of developing the electrical and mechanical sections of the model, prior to solving the WRI rolling contact equations, required a temporary wheel-rail adhesion characteristic. This is provided by a curve-fit of the typical curve examples shown in Figure 3. Each curve has evolved by data assimilation from various sources [2, 3, 4] to eliminate the risk of biased data due to atypical or erroneous measurement. These empirical curves are very non-linear, so a piecewise linear model approach was effective and readily implemented within Spice functions [5]. The initial steep positive slope is relatively linear and a straight-line representation is acceptable for development purposes prior to contact patch modelling. However, slip and creep operation is crucial to this study, therefore initial model testing also relied on realistic friction behaviour beyond the initial steep slope.

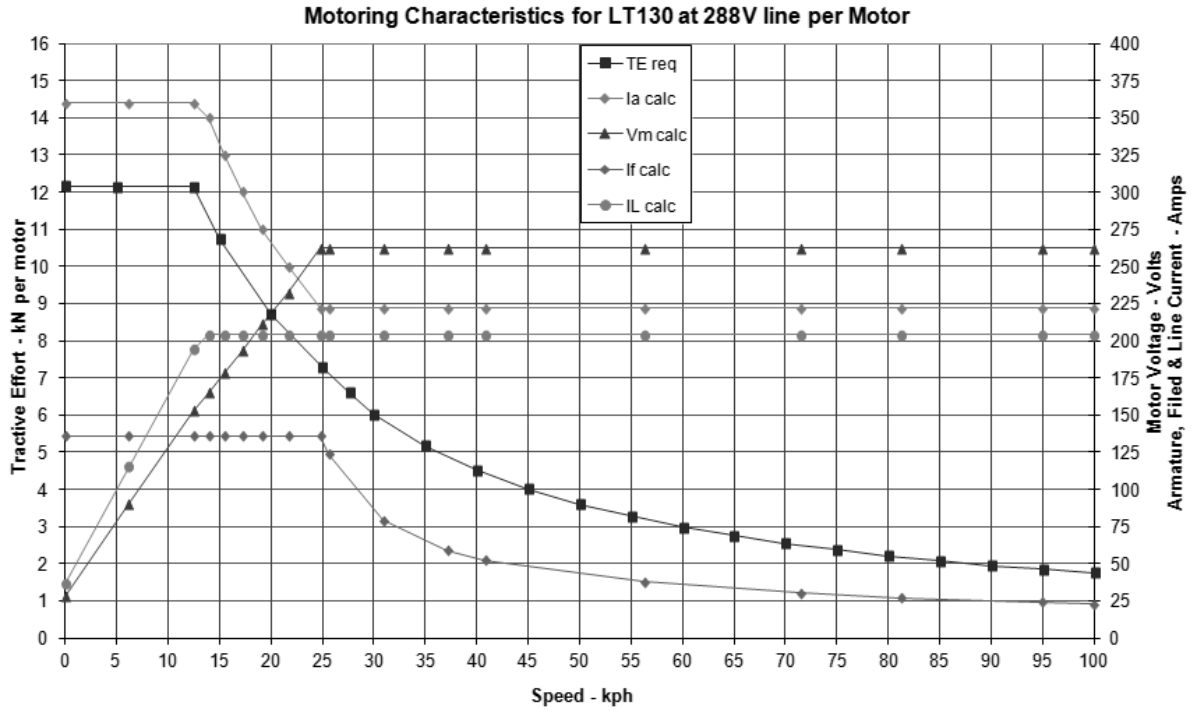

Figure 1 92TS Motor (LT130) Characteristics - Maximum TE and Armature Current is from 0 - 12kph with Field-Weakening commencing at 25kph. Curves are for nominal 680mm wheel diameter.

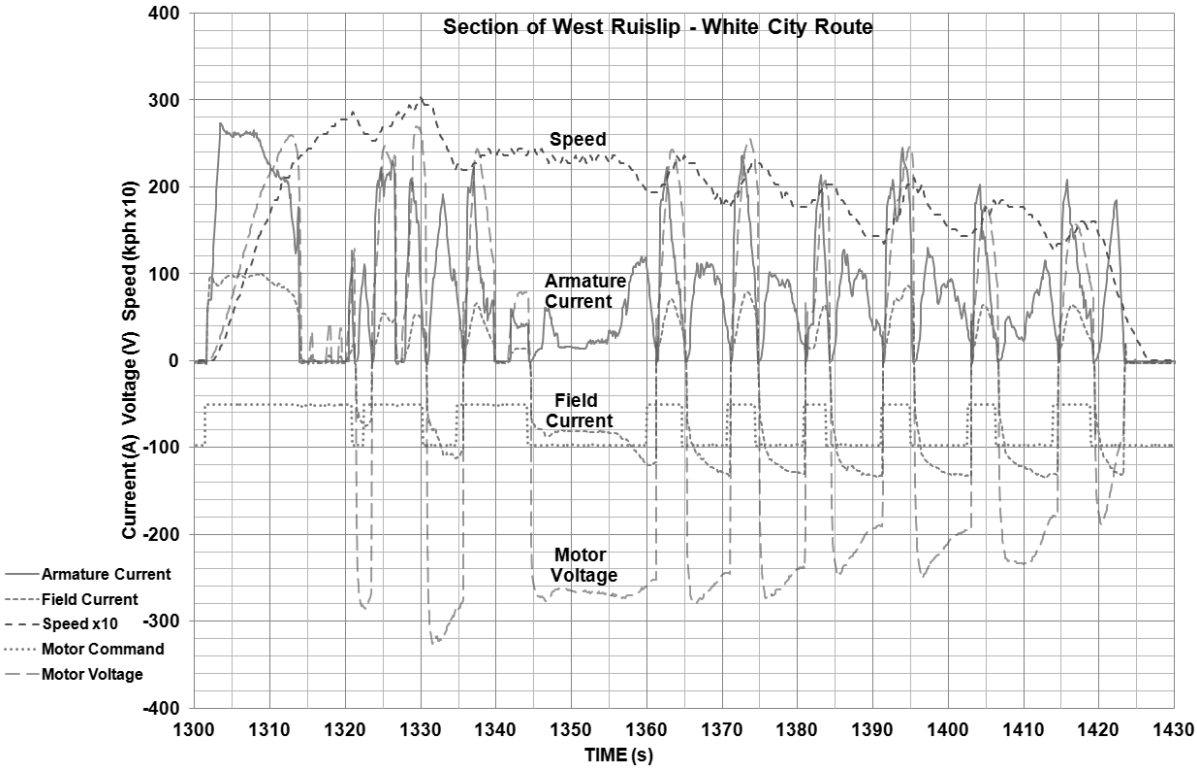

Figure 2 Typical Operation in Traffic with repetitive bursts of low speed Motor-Brake cycles

At a later stage in model development the adhesion curves were replaced by a WRI model that includes Hertzian compression, a dimensioned contact patch, tangential and lateral forces and stresses [6]. The friction coefficient is profiled to reflect realistic changes in rail condition and the effects of rail profile and depression between sleeper supports are included. Importantly, the mathematical WRI solution provides the rail surface forces and stresses required to predict energy dissipated by the wheel and rail at the contact patch.

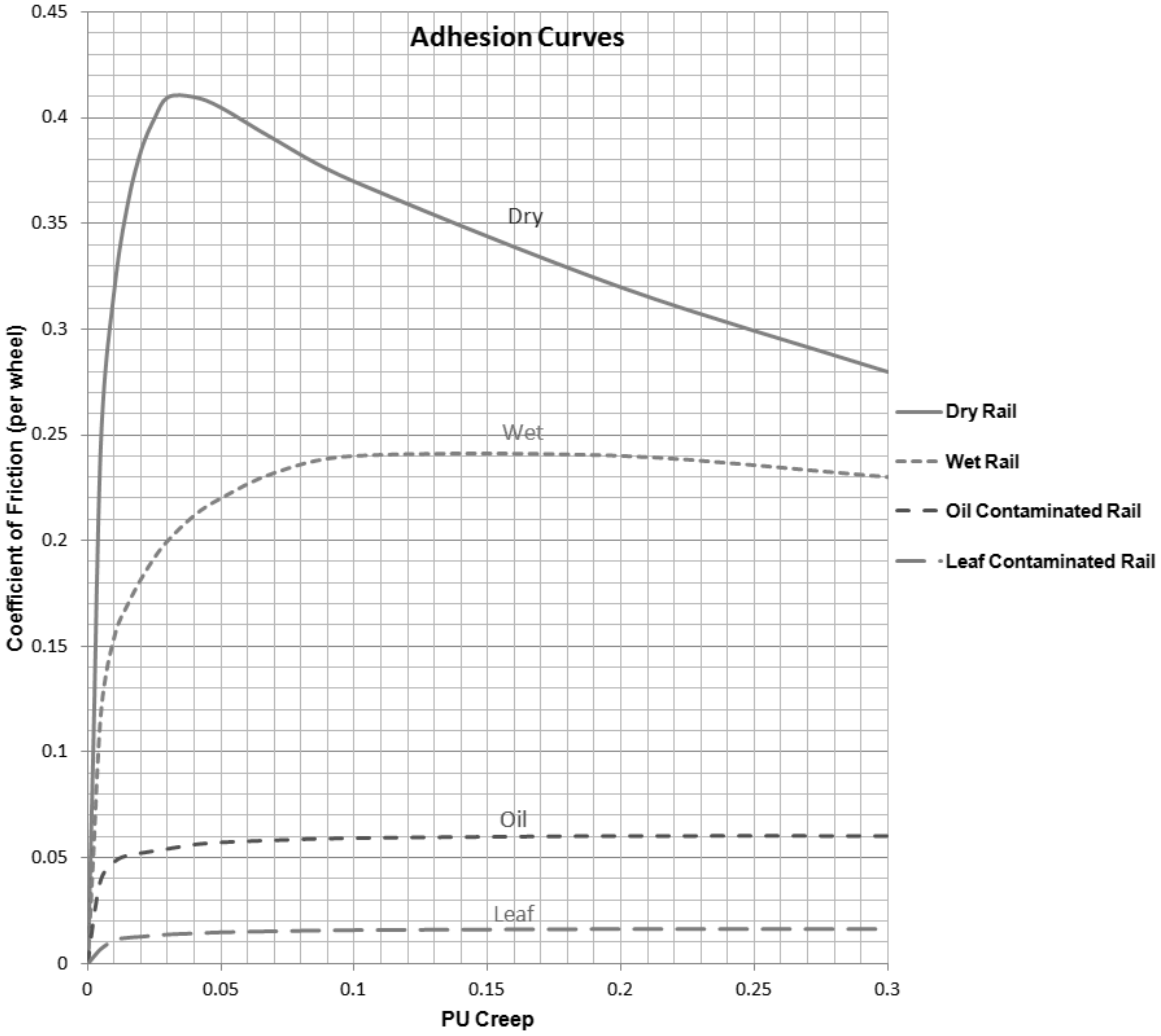

Figure 3 Example Adhesion Characteristic experienced at the WRI for differing Track Conditions

1.3 Patterns in Defect Location

The outcome of initial investigation using ultrasonic detection of defects raised the following questions:

1. Why do defects only occur on surface sections?
2. Why are lines only operating traditional series motor DC fleets unaffected?
3. Why are there few occurrences in platform grounds?
4. Why some surface locations are significantly affected while other areas remain unaffected?

The highly probable explanation for the first question is the influence of external environmental factors on rail condition and thereby on defect generation. For example, surface section rail adhesion conditions are much more variable than those in underground sections, which are also commonly higher due to absence of environmental contaminants. Combining this conclusion with the deduction from the second query that modern, as opposed to traditional, rolling stock features in defect causation, leads to a probable scenario that the modern traction control response to low and/or varying levels of adhesion is an important factor.

Drawing firm conclusions from the third and fourth questions was less easy. A map of Central Line affected areas was drawn up to search for localised defect patterns. A representative sample is depicted in Figure 4, where thick solid lines highlight seriously affected areas and checked lines shows areas which would commonly be susceptible to congestion or restricted running. The absence of platform regions implies that the problem does not occur when accelerating from standstill to 10kph, but only once the vehicle is moving. Finally, it is plausible from the highlighted regions that correlation with areas of frequently congested traffic flow is a factor. In a congested condition the train speed is lower than normally expected and ATO functionality cycles the traction through periods of maximum acceleration and braking to regulate the traffic flow. Figure 2 is an example of such behaviour where the dashed line speed trace indicates the speed variation against time in seconds.

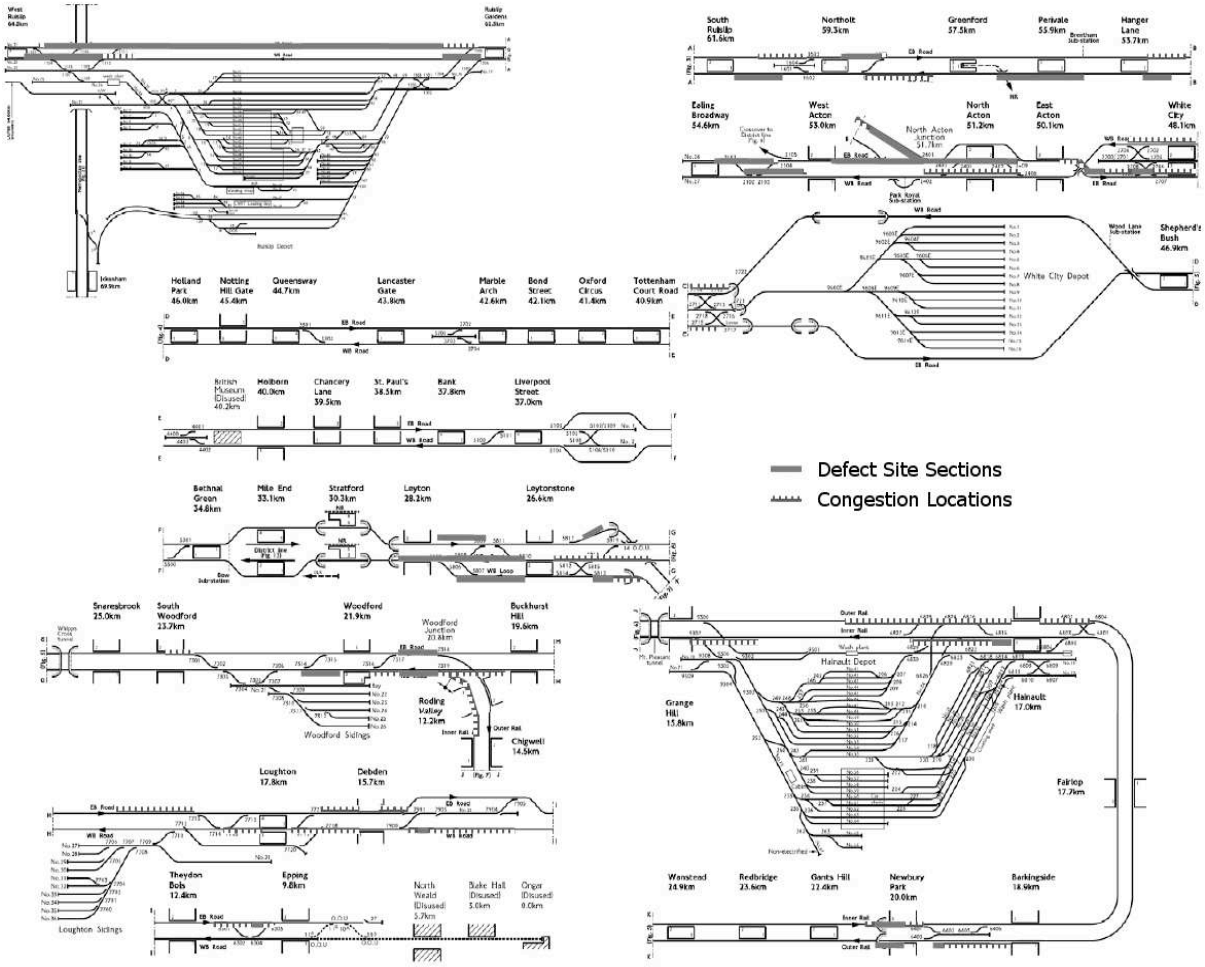

Figure 4 Central Line Map indicating Defect Areas and Congestion Locations

2. PHYSICAL EVIDENCE FROM RAIL EXAMINATION

The next stage of the investigation was a detailed examination to reveal the state of rails at typical defect sites. The rails investigated were taken from the Central Line, and the examination followed a similar strategy to that used with rails from the Northern Line examined previously [7] to which the reader is referred for details of the methodology.

2.1 Visual Inspection

Rails were removed from four sites at which ultrasonic inspection had identified cracks, and at which visual appearance and the distribution of defects suggested the new squat damage mechanism was active, rather than conventional squat development. Nital etchant (nitric acid in ethanol) was used externally on the rail heads to identify the location of white etching layer (WEL) and find out how it related to visible plastic flow and crack mouths. The conclusions of the examination were:

- Ultrasonically detected defects were associated with shallow surface depressions on the rail surface. Multiple additional shallow depressions were usually present along the stretch of rail in which the ultrasonically triggering defect had been found.
- Spacing between adjacent surface depressions was around 50mm.
- Patches of white etching layer were present with similar spacing to the shallow surface depressions, suggesting a periodic heat input.

2.2 Crack morphology and interpretation

Following external examination, the rails were sectioned in the longitudinal direction, parallel to the running direction, and approximately mid-way across the running band. No attempt was made to locate the deepest region of the defect (for example by eddy current technology) as it was thought this approach was sufficient to gain understanding of the internal structure of the defects. It was discovered that:

- The largest cracks were at each of the ultrasonically identified defect sites, reaching depths of up to 7mm. Other surface depressions had much smaller if any evidence of cracking.
- The material at the rail surface had only very slight or no evidence of plastic deformation.
- WEL was present directly above or very close to the main cracked regions.
- The WEL thickness was in the range 50 to 125μm in areas close to cracks. WEL of this thickness is at the very high end of the thicknesses previously reported internationally within the industry [8,9] and is indicative of significant heat input to the rail.
- Crack lengths up to 75mm were observed.

Figure 5 uses a series of stitched micrographs to show a typical large crack at one of 6 ultrasonically detected defects within a 6 metre length of rail (code UC10010). Many more shallow surface depressions were present between these six more fully developed defects. At the top of the figure thick black lines indicate the position of white etching layer on the sample surface, showing that it lies directly above the crack. The crack itself is closest to the surface near to the WEL, and has propagated down in both forward and reverse directions along the rail. The right-hand region of the crack has a series of fine upward branches and the tip of the crack has dispersed into an array of fine cracks, whereas the left side crack has not branched. Although the crack does not break the surface on this cross-sectional plane, evidence from other cracks in the sample is that they would break the surface either on a plane further 'back' into the rail, or in the material which has already been cut away to take these micrographs.

Figure 6 shows a detailed view of the WEL for the same crack as in Figure 5. Here, etching the surface with nital has revealed in the pro-eutectoid ferrite (shown as a white network) surrounding the pearlite, which makes up the bulk of the rail. These white lines are useful markers and their undisturbed state across the sample indicates that there has been very little plastic deformation, either at the surface, or on the crack faces. Even within the WEL the pattern of undisturbed pro-eutectoid ferrite remains, indicating that the transformation of the rail surface to WEL has been a thermal process rather than the result of mechanical work.

A final sample from rail UC10010 was taken at one of the shallow surface depressions that had not developed into an ultrasonically detectable defect at the time of rail removal from track. Figure 7 shows that a very shallow surface crack has formed directly below a region of white etching layer. There is little or no evidence of plastic deformation, which is remarkable given the lack of support for the thin sliver of material above the crack. In many mainline rail cases it would be expected that plastic flow would develop at the rail surface, and this would become extensive in material undermined by cracking.

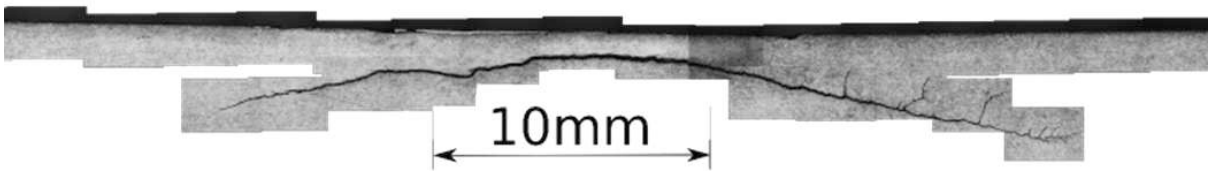

Figure 5 Site of ultrasonically detected defect in rail UC10010. A patch of white etching layer lies directly above a crack, which does not break the surface on this cross-section of the rail. The crack is growing down into the rail to both the left and right of the white etching patch. To the right the crack forms a series of branches up towards the rail surface.

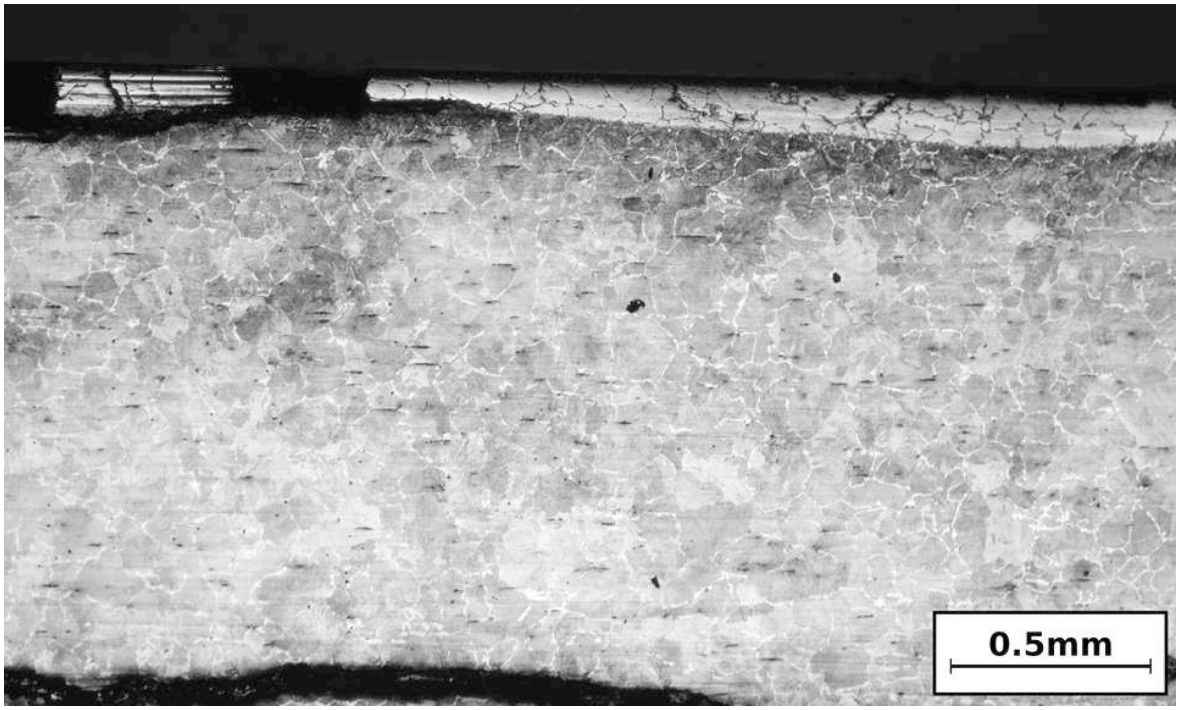

Figure 6 Detail of white etching layer in Figure 5, rail UC10010. Thickness of the layer is approximately 125μm at its deepest point. The microstructure shows very little plastic flow, either at the surface, or on the boundary of the crack at the bottom of the figure. The ferrite of the original microstructure remains visible inside the white etching layer.

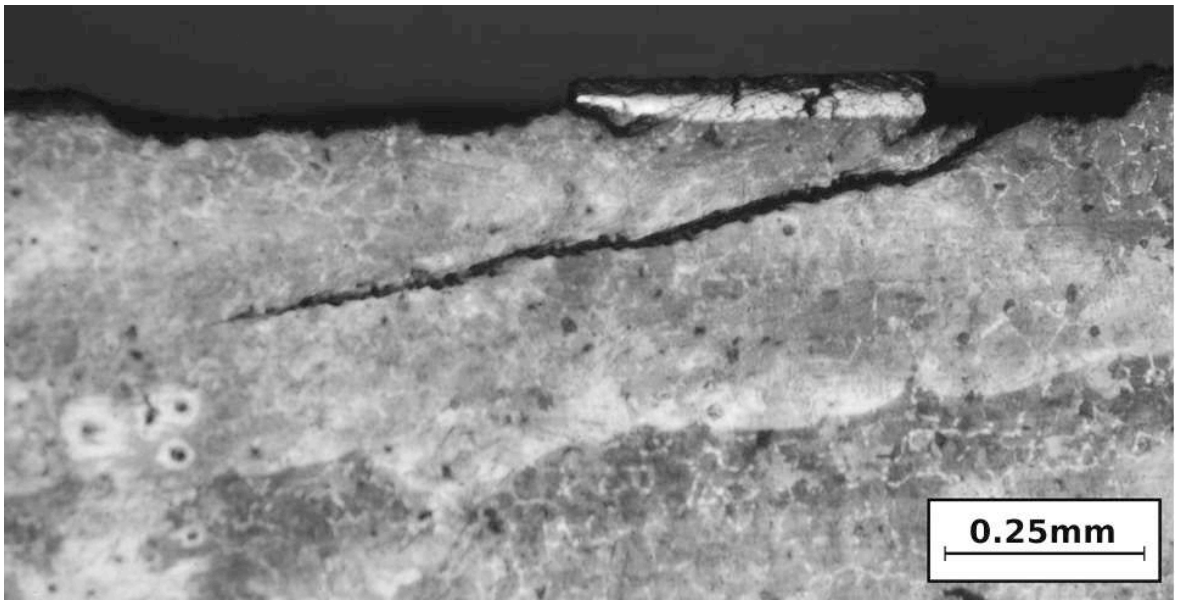

Figure 7 Detailed view of the small patch of white etching layer above an inclined surface breaking crack away from the major defects in rail UC10010. To the left of the white layer some of the rail surface has been lost, possibly through break-away of additional white etching layer. There is very minimal plastic deformation in the material.

2.3 Crack Growth and Site Monitoring

Crack initiation in rails is often attributed to the ratchetting process [10] through which plastic damage accumulates with each passing wheel. Crack formation or the generation of wear debris follows, as accumulated strain reaches a 'ductility exhaustion' point, and in some cases cracks progress to propagate to dangerous lengths. Evidence from the current rail samples (Figure 5 to Figure 7) and from previous investigation of similar defects on the Northern Line [7] shows that there is very minimal plastic flow present, and the ratchetting mechanism could not account for the initiation of cracks. The evidence of Figure 7

showing a small crack just below a region which has been transformed by heat is more supportive of a thermal crack initiation mechanism rather than the conventional ratchetting mechanism.

Whatever the initiation mechanism, the shallow inclined near surface cracks of the type in Figure 5 have similarity in appearance to many rolling contact fatigue cracks. The major mechanisms thought to be responsible for rolling contact fatigue crack propagation are shown schematically in Figure 8. Relevant to the current study is that the major cracks observed had no evidence of plastic flow near the crack faces which would be typical of most rolling contact fatigue defects. The motion and rubbing of the crack faces as they grow usually smoothes the faces and produces plastic flow in the adjacent material, but this plastic flow and smoothing is not present in the rail defects observed here. It is not suggested that the cracks have appeared 'fully formed' or spontaneously, and possibilities for what drives crack propagation include:

1. LU rail-wheel contacts are generally low pressure relative to mainline railways. Cracks may be growing by a conventional mechanism (Figure 8), but with such slight movement and under very low compressive load so the surrounding material is not deformed.
2. The growth may have a thermal mechanism, which has never previously been associated with standard fatigue defects. The mechanism and growth rate of the thermally initiated defects is the subject of a separate study [11].

A controlled trial on Central, Northern and Jubilee Lines has allowed some defects to be left in situ and monitored ultrasonically to ascertain growth rate. Results are being compared to the established growth process of standard rolling contact fatigue cracks shown in Figure 8. This has confirmed that growth is not sudden or immediate, but cannot provide evidence for the growth mechanism driving the 'squat type' defects. However, it is also likely that the growth mechanisms depicted in Figure 8 remain influential in the propagation of thermally initiated defects.

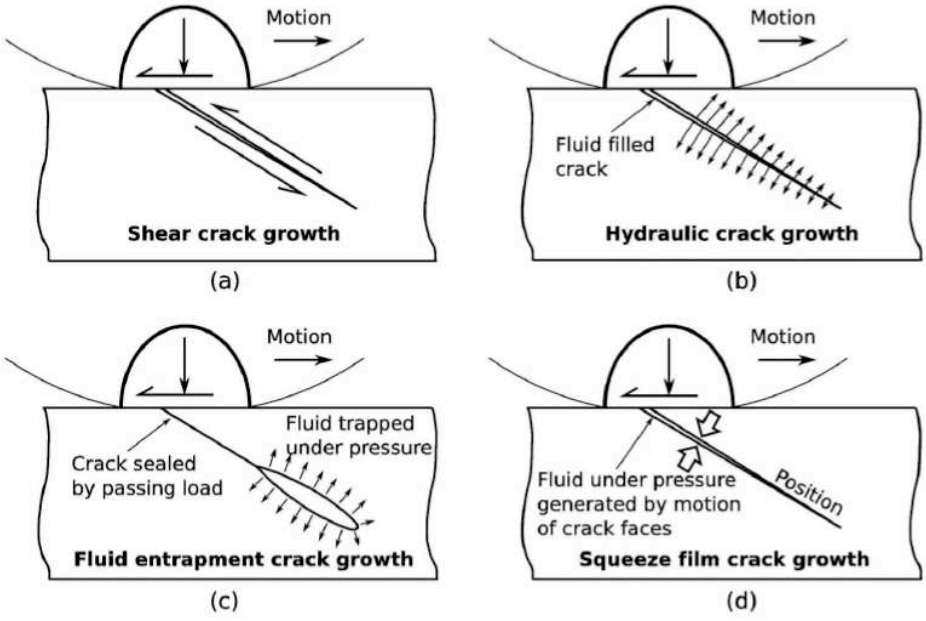

Figure 8 Schematic representation of Rolling Contact Fatigue crack growth mechanisms

3. TRACTION CONTROL SYSTEM MODELLING

The metallurgical evidence that defects are associated with thermal stress and rail surface transformation provided essential new information to direct the traction modelling study. It was proposed to develop a portable 2-car 92TS traction model. The model would include transmission, suspension, and track dynamics to facilitate understanding of the track forces and stresses involved at the wheel-rail interface (WRI) and their response to traction events [12]. It was uncertain at the outset if such extensive combined electrical, mechanical, behavioural, and physical modelling of a 2-car train and track section was feasible within a single modelling platform. The model was created around the traction electrical and power electronics with closed loop armature and field current control of the separately excited DC motor system with wheel-spin control.

3.1 Requirements and Assumptions

The modelling objective was to investigate potential defect scenarios and understand the interaction and sensitivity of traction performance to contact patch size, as well as tangential force and stress. The model is based on the well established and proven Spice circuit simulator package with input schematic capture. Hierarchical and behavioural (math based) modelling principles are available to handle complexity issues faced in both electrical and mechanical dynamic systems, as well as solving the non-linear rolling contact equations. An innovative aspect of the model development was the capability of the Spice platform to adapt to multi-disciplinary functions, not only electrical systems for which it is reputed and intended. Alternatively, a multi-discipline simulator such as Matlab could be applied to the modelling problem. However, the more portable solution offered by Spice was preferred.

The 2-car propulsion system comprises 8 individual motors and running gear, 16 WRIs, 4 separate armature choppers, a field chopper, a line filter, 4 associated armature control systems and a common field control system. The motor model had to accurately incorporate the non-linear magnetising characteristics of flux saturation and armature reaction to produce realistic electrical behaviour.

The model of the traction wheel-spin control located within each armature control system is driven from wheelset based velocity and acceleration differences between motored and trailer bogies. This critical part of the system model made use of real-time software equations transferred into Spice to ensure accurate reproduction. Based on prevailing rail conditions, the wheel-spin system may operate for considerable time whilst restricting creep. This is effectively a quasi-creep controller, which reduces the applied TE by that necessary to satisfy and sustain a creep limit criteria (nominally 3kph). However, this type of control does not seek the adhesion peak, but instead prevents excessive creep developing. It works on the principle that the creep limit is invariably set beyond the creep at which peak adhesion is expected and that any shallow negative slope after the peak will not result in significant performance loss. These are reasonable assumptions for passenger rolling stock on well maintained track.

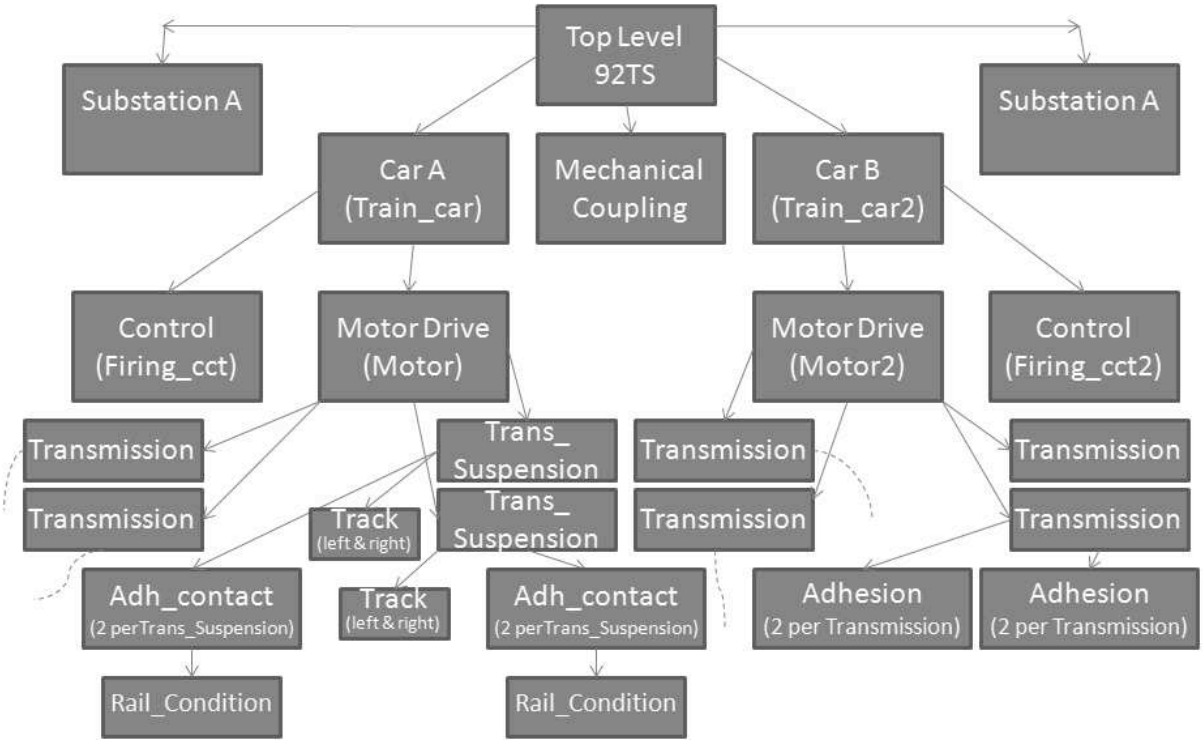

Figure 9 Structure of 92TS Traction Model from Substation to Track including WRI

(Dotted lines indicate paths to duplicated subsystems omitted for clarity)

The mechanical powertrain subsystem model (Figure 9, Trans_Suspension block) is augmented by a damped Hertzian contact stiffness (Figure 9, Track block) to reflect correct vertical contact depression and dynamic response of the contact patch (CP) to rail corrugation and track based sleeper stiffness perturbations. The core of the model is the rolling CP representation (Figure 9, Adh_contact block), which is assumed non-conformal for efficient solution. To improve execution time only the 4 WRIs on the leading bogie need to include the full CP, while the other bogies use a simpler transmission model (Figure 9, Transmission and Adhesion blocks) based on an appropriate empirical adhesion curve (Figure 3).

3.2 Simulation Development

The optimum system model is a combination of modelling styles and methods. It can be summarised as a need to minimise an objective function comprising:

- Model complexity due to interacting electrical / control / mechanical / physical specialities.
- Inclusion of pertinent dynamics - accurate transient response at the WRI is important.
- Inaccuracies in Hertzian contact and non-conformal contact patch solution.
- Practical execution time.

These are conflicting objectives, made critical by the integration tolerance rigour necessary to achieve a continuous convergent solution for each CP across multiple WRIs. Therefore, the problem was initially simplified by sub-division into three separate tasks:

1. Modelling of wheel-spin control, transmission and suspension elements using an empirical adhesion curve as substitute for the CP model; run the model to prove each element worked correctly, validating the model against measured motor electrical characteristics where possible. The primary suspension longitudinal and vertical dynamics were included, but secondary suspension has insignificant influence and was not modelled.
2. Development of track and WRI models that interface to the CP; run the updated model to establish that these aspects produced expected behaviour and credible predictions. The track model transfers the bogie normal load to the rails incorporating sleeper base variations and Hertzian hysteresis damping. These modes are modelled as interacting spring-mass-damper systems using Spice maths capability employed to build representations of differential equations.
3. Modelling of the CP equation set and its integration into the simulation by replacement of empirical adhesion curves. Test of the complete simulation by running of initial scenarios (sets of vehicle TE, speed, and rail conditions) to confirm expected CP dimensions against results in [13], track stresses and forces, and credible values of Tgamma, where Tgamma (also referred to as $T\gamma$ or wear number) is the product of tangential creep force and creepage, commonly used as a measure of energy dissipation at the WRI.

The CP equations based on the Polach [13] non-linear creep force model are implemented in 3 dimensions by the simplified theory of wheel-rail rolling contact due to Kalker [14]. This permits future model extension, unlike abbreviated longitudinal-only theory, but requires an exceptionally computation efficient solution to Kalker's rolling contact theory. This is achieved using non-linear equation-based, behavioural Spice version 3 math sources evaluated by Newton-Raphson successive approximation. The complete solution includes the following processes;

- A closed solution to Hertzian stiffness and contact compression determined using math function sources.
- The output of the Hertzian computation provides the contact ellipse dimensions as input to Kalker's lookup tables, to decide coefficients C1, C2 & C3 to be used within the CP solution. Kalker's coefficients are used in wheel-rail contact theories to determine the tangential forces and spin moment.
- Polach equations determine the tangential forces based on C1, C2, C3 and a CP elliptical surface mapping of the static Hertzian stress distribution to a linear gradient stress over the adhesion region (Figure 10).

The Polach CP solution involves several assumptions, all proving acceptable to the modelling objectives of this study. These include a locally constant coefficient of friction (μ), thus restricting any variation in adhesion within CP dimensions. Polach also developed solutions with friction coefficient dependence on slip velocity [15], effectively allowing variation of friction coefficient across the contact patch, but these are not used here. The

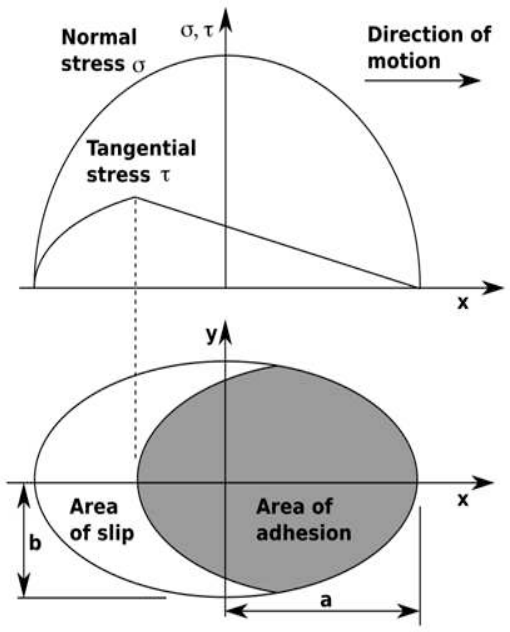

Figure 10 Contact Patch Ellipse with Stress Distributions

contact area must be divisible into two distinct and separate areas of adhesion (stick) and slip. The maximum tangential stress equates to μ times the normal stress, with a linear increase of tangential stress from the leading edge of the adhesion region. The accumulative error [16] in the resulting output forces, due to the assumptions of the simplified theory does not exceed 15%.

The inputs to the CP/WRI model are the normal load (dynamic, time-varying, individual per wheel), μ, wheel modulus of rigidity, ellipse semi-axis dimensions (a & b from Hertzian contact compression solution), Kalker's coefficients (implemented by lookup tables within model), longitudinal and lateral creep (from model dynamics), and spin creep (turning motion, set to zero for this investigation as no evidence to correlate defect incidence with curves). The outputs are the longitudinal and lateral forces, which also feedback into the traction model to determine resultant drive dynamics. Figure 10 represents the CP ellipse produced by the Hertzian solution, symbolically with the major radius in the direction of vehicle motion. In practice, metro rail system parameters often result in a major semi-axis in the lateral direction with radius in the range 5 to 18mm. The minor semi-axis radius is significantly less, with typical range 2 to 7mm.

3.3 Model Predictions

The model is run for commonly occurring levels of adhesion from 12% to 30% and for sudden adhesion changes within this range. The model can operate over the whole vehicle speed range in both motor and brake. However, it is only motoring at low speed, below 20kph, where required TE exceeds the available adhesion for operation towards the lower end of the typical 12-30% range. It is useful to emphasise the definition of adhesion, as the ratio of tractive to normal forces transmitted at the wheel-rail contact. This is distinct from the friction coefficient which represents the maximum available adhesion, which is often creep velocity dependant, as illustrated by some curves in Figure 3. The results in Figure 11 show the effect of transition from 12% to 30% adhesion on the leading bogie (string 1) under maximum acceleration at 12kph. The trailing bogie (string 2) operates at 30% adhesion throughout.

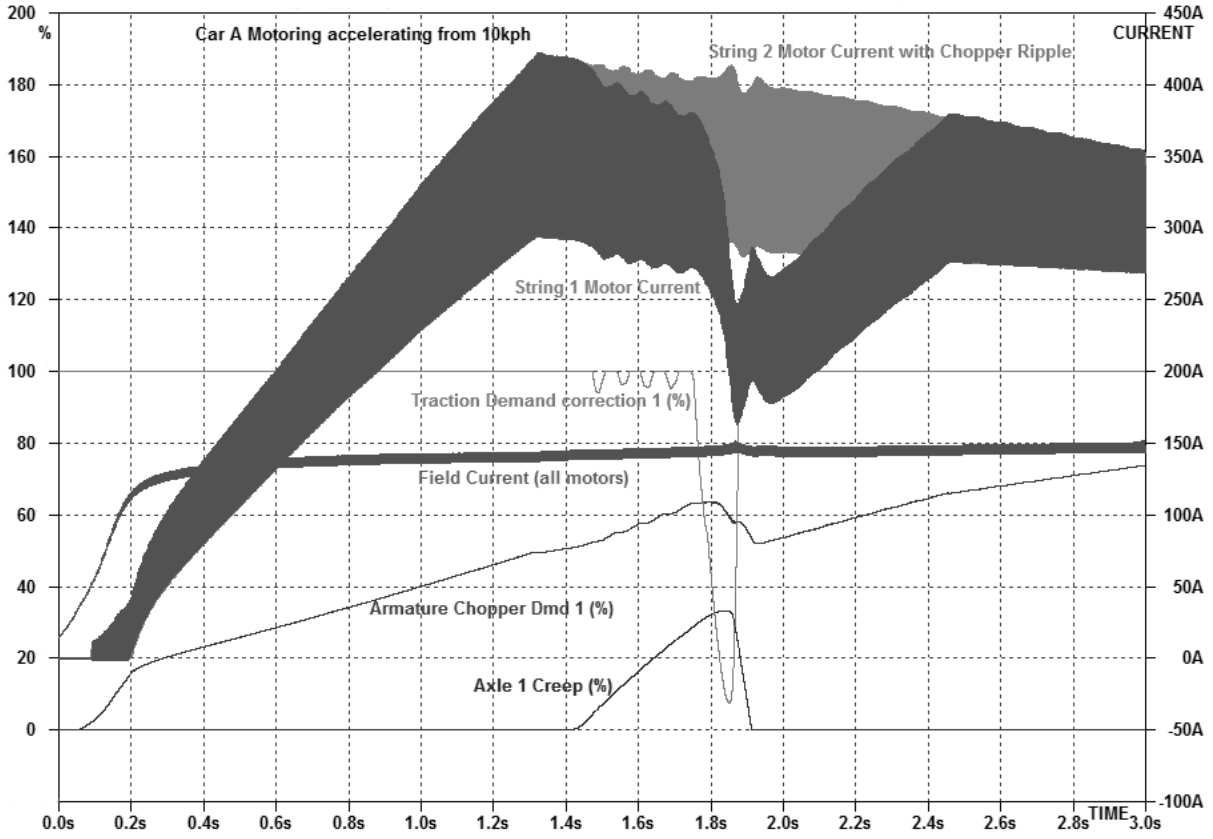

Figure 11 Predicted acceleration performance of 92TS Control System encountering wheel slip at 12kph

The low adhesion is only experienced on the leading bogie (denoted number 1) until approximately 1.9s, when the coefficient of friction suddenly increases (for example, if the wheels have moved from wet to dry rails). The trace of motor current string 1 is reduced (compare with trace of motor current string 2) in an attempt to correct the developing creep over the period 1.3 to 1.9s, limiting it to just over 30% (Axle 1 Creep trace). The resulting corrective action of the armature chopper demand is shown in percentage terms, with 100% representing chopper full-on. The field current is common to all motors and is effectively

unchanged by the corrective action. After adhesion is recovered (when the creep falls as the wheels moves back towards a rolling condition with only micro-creep) the armature controller for string 1 ramps the current back up to the required demand.

Any mode of operation producing an unusually high contact patch stress is of particular interest in this study, since this could potentially produce the surface rail energy and temperature rise required to initiate the squat type fatigue events. Throughout modelling the right and left rail tangential stresses are individually computed as the mean value across their respective adhesion contact area. A single adhesion recovery event as described above will normally occur as the tractive effort demand is reduced when operating under a wheel-spin control regime. However, the simulation has enabled identification of a more severe situation, which exists when the traction wheel-spin control system operates in quasi-creep control where the adhesion level is only just below that required for full TE (this occurs regularly and is more likely at low speeds). As with the Figure 11 scenario, this severe situation occurs due to a sudden improvement in rail condition as re-adhesion from controlled creep operation is rapidly recovered.

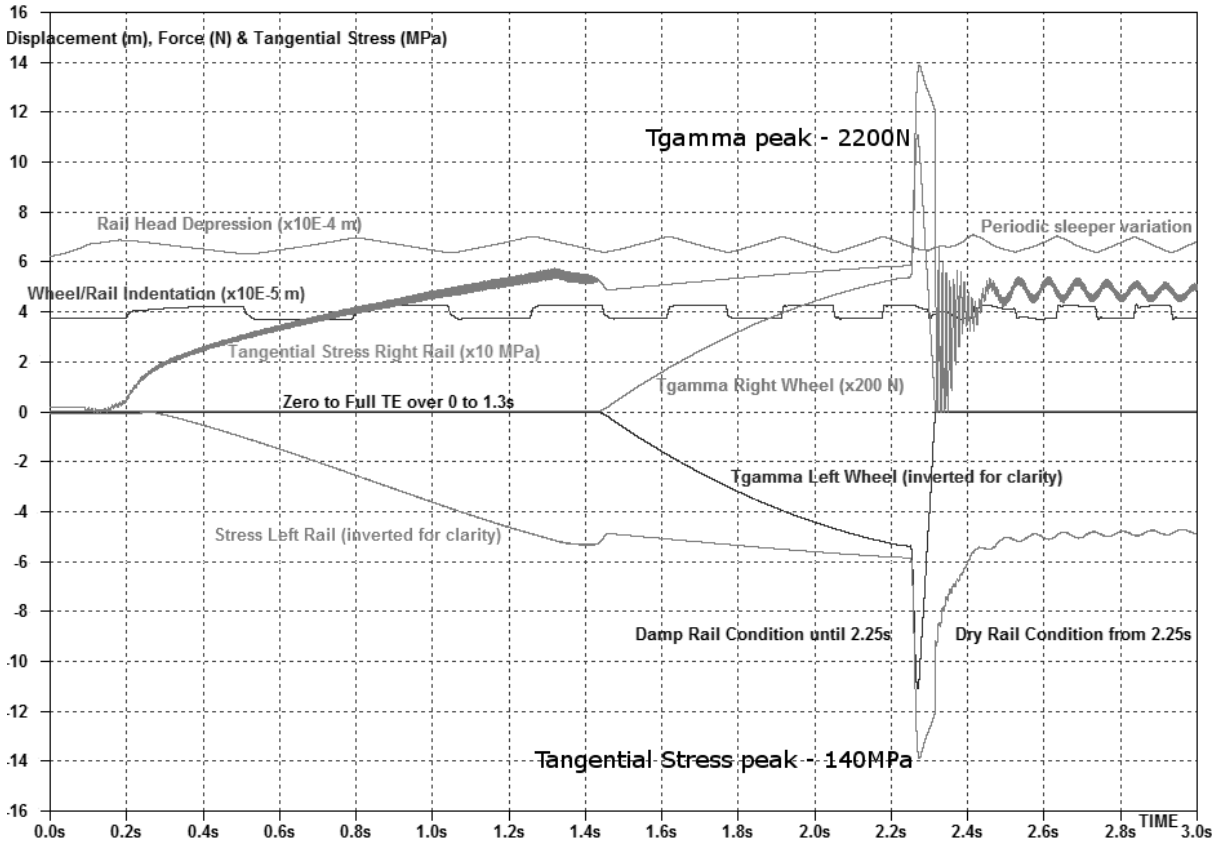

Figure 12 Simulation results for re-adhesion (14% to 30% at 2.25s) after a period of creep control limiting. Re-adhesion peak tangential stress pulse is 140MPa, almost three times the usual maximum acceleration value, with corresponding very high energy Tγ value exceeding 2200N.

The resulting transient process at the WRI produces a high tangential force and stress. Because of high initial acceleration requirements, this condition can occur frequently when the rail condition is degraded, for example, due to minor surface contamination or dampness. On transition from damp to dry (or good) rail condition, illustrated at 2.25s in Figure 12, the available adhesion suddenly increases. The wheel-spin control action ramps to the demanded TE as the creep reduces to a small value required to deliver the accelerating tractive effort. In the process a considerable mechanical transient is produced as the creep recovers over the peak point of the adhesion characteristic (consider dry rail curve in Figure 3). This transient behaviour produces peak rail surface stress and Tγ values, potentially sufficient to risk initiation of CP thermal damage.

Figure 11 and Figure 12 indicate adhesion recovery for a sudden adhesion increase. However, recovery of an inertial wheelset and transmission takes a finite time. Similar tangential stress and Tγ peak values will still be experienced provided the improving adhesion rate of change exceeds the inertial recovery rate.

From observation there is no significant damage to the wheels on the trains, so wheel spin rather than slide is considered the probable source, since under sliding conditions the wheel would become hotter than the

rail and exhibit greater damage. All three fleets have wheel slide protection systems, which function adequately and prevent significant wheel flat generation. The degree of wheel spin required to produce a defect does not need to be exceptional. This is supported from evidence that the martensite layer formed by a wheel 'burn' event is generally significantly thicker than that observed on the samples analysed. Also, the locations (near station platforms) that would be most susceptible to wheel spin from rest appear to be almost unaffected by the problem. Based on this, the likely origin of the defects is as a result of wheel spin at low but non-zero speeds. This theory was substantiated by thermal modelling results of section 4.3.

The traction model suggests that a possible cause of the phenomenon is the combination of changing rail condition and the nature of low speed traction wheel-spin control, which by quasi-creep control operation functions well beyond the adhesion peak for considerable periods under degraded adhesion conditions. This differs from more traditional wheel-spin systems that reset to a low effort as soon as slip is detected, thus regaining adhesion before significant creep levels develop. Such traditional systems are found on DC series motor rolling stock and are inferior in terms of efficiently utilising available adhesion, but they avoid protracted operation at creep levels beyond the adhesion peak. As a consequence, with DC series motors high stress recovery events are not likely to occur unless the loss of adhesion is very severe, causing the creep level to increase more quickly than the wheel-spin controller response. Unlike modest reductions in adhesion due to damp or lightly contaminated rail, such severe adhesion loss only results from serious rail contamination, which is uncommon.

4. RAIL-WHEEL CONTACT THERMAL MODELLING

The traction-WRI modelling has provided an indication of the CP energy expected during 92TS low speed adhesion recovery resulting from a sudden improvement in rail condition. Thermal modelling was then used to interpret the effect of the CP input energy on the temperature of the rail.

4.1 Assumptions

Crucial to the modelling was the temperature variation over time required to produce a white etching layer on the surface of a steel rail. The following assumptions about WEL properties on LU track were made.

- WEL found on the surface of rail defects is martensite formed by thermal transformation.
- Martensite WEL forms when the steel is heated to above 727°C (this is the eutectiod temperature for an iron-carbon compound) and cooled in around 1 second or less to below 500°C, and then to a temperature at or close to ambient[17]. Exact times and temperatures will vary slightly with steel composition.
- Friction and sliding at the WRI causes both rail and wheel temperature to rise, but energy flow depends on existing temperatures and is not necessarily equal to both bodies.

4.2 Thermal Models

A range of thermal models are available for CP interaction, with many linked to research in the 1950's by Carslaw and Jaeger [18]. These early models are "steady state" implying that they can only be used to model wheel spins or slides exceeding half to one second duration under constant conditions. Taking into account the train speeds and transient nature of the defect generation mechanism of interest, it was decided this could not be analysed satisfactorily using these models. Initial calculations with a limited slip model by Ertz & Knothe[19] showed that the resulting steady state temperature rise of the wheel would only be around 100 - 150°C, far less than that required for WEL formation.

A model for transient sliding of a wheel was developed by Sawley [20], originally for wheel and rail temperature prediction in wheel slide caused by a locked wheel on a moving vehicle, i.e. "gross sliding" of a wheel on a rail. This model describes a 3D contact, and enables prediction of contact temperature and variation of temperature with depth into the rail and wheel. It also provides a means to calculate how contact energy is apportioned to the wheel and rail, and how this varies over time as the component which is stationary relative to the contact heats up. The model was originally developed for a sliding wheel, whereas the current situation is wheel spin, so the model was applied by effectively reversing the position of the rail and wheel components. It is a transient model, able to predict temperature change as a slide begins to take place, before steady state is reached, assuming the worst-case of a spinning wheel with no forward vehicle motion. The model is not able to take account of contact geometry change during sliding, and assumes material properties are invariant with temperature. Overcoming these assumptions would require development of a much more comprehensive model, and this was beyond the scope of the investigation.

In both the Sawley and Ertz & Knothe models the rail-wheel CP is a frictional source of thermal energy. The relative slip speed between rail and wheel determines the thermal input level. The surface temperature of the

rail and wheel in the CP are assumed to be equal since they are under such close and high pressure contact. How the thermal energy is divided between the rail and wheel depends on their individual speed relative to the contact patch and their thermal properties. Effectively, energy flows to heat the cooler steel as it enters the contact patch to match the temperature of the hotter component. The division of energy flow can change rapidly when spin takes place, starting from approximately equal amounts into rail and wheel. This results in short impulse temperature rise at the CP, which is superimposed on any long term steady state increase in temperature.

Quantity	Value
Thermal conductivity (K), W/mK	35
Thermal diffusivity (ϕ), m^2/s	$1.10 * 10^{-5}$
Contact half dimension (equal in lateral and longitudinal directions), mm	4.25
Contact load, kN	30
Surface friction coefficient	0.05, 0.1. 0.2, 0.3

Table 1 Thermal properties of Rail and modelling Parameters

Table 1 gives the thermal properties of the materials modelled, with properties assumed to be identical for rail and wheel. Also given are the contact size, load and friction conditions modelled, which were based on typical output from the vehicle modelling. In future it may be possible to conduct the thermal modelling to include changes in contact patch size and load over time, but for the current work these values were held constant for each run of the thermal model. Thermal conductivity is itself temperature dependant, but the model was unable to consider this variation, and a value corresponding to a temperature of around 600°C was chosen as this corresponded to around the expected temperature reached at the wheel-rail interface[21].

4.3 Results

Both Sawley and Ertz & Knothe models consider frictional energy input due to creep in the contact area, however, the available input energy data is in the form of Tγ values. These can be linked if the surface power density q_0 is defined in terms of normal load N, friction coefficient μ, sliding velocity V_{slide}, and contact area A.

$$q_0 = \frac{N\mu V_{slide}}{A} \tag{1}$$

The tractive force is equal to the normal load multiplied by the friction coefficient

$$T = \mu N \tag{2}$$

And the slide velocity is equal to the vehicle velocity multiplied by creepage

$$V_{slide} = \gamma V_{vehicle} \tag{3}$$

Combining (2) and (3) into (1) the thermal input can be defined just in terms of Tγ, vehicle speed and contact area. Hence, CP power density is given by

$$q_0 = \frac{T\gamma V_{vehicle}}{A} \tag{4}$$

Extracting numerical values for the simulation result in Figure 12, Tγ=2200N, $V_{vehicle}$ = 3.75m/s, and A = 0.0001m^2. Therefore, q_0 = 82.5W per mm^2 and the power dissipated within each CP = 8.25kW.

Thus, thermal modelling links Tγ to power density and consequently temperature rise, giving a connection between wheel (and preceding vehicle) dynamics and rail-wheel temperature rise. The Sawley model is adapted here to represent a spinning stationary wheel, whereas the real cases of interest are of a wheel spin on a slowly moving vehicle. The temperatures predicted must therefore be interpreted carefully, but will be close to those reached for the duration of a contact area passing a specific point on the rail surface. A simple check on the temperature prediction is that the physical evidence is of WEL formation, but not of melting of the steel. This gives a window of 727°C to around 1400°C, which aligns well with the predictions for an appropriate range of vehicle speed and contact conditions.

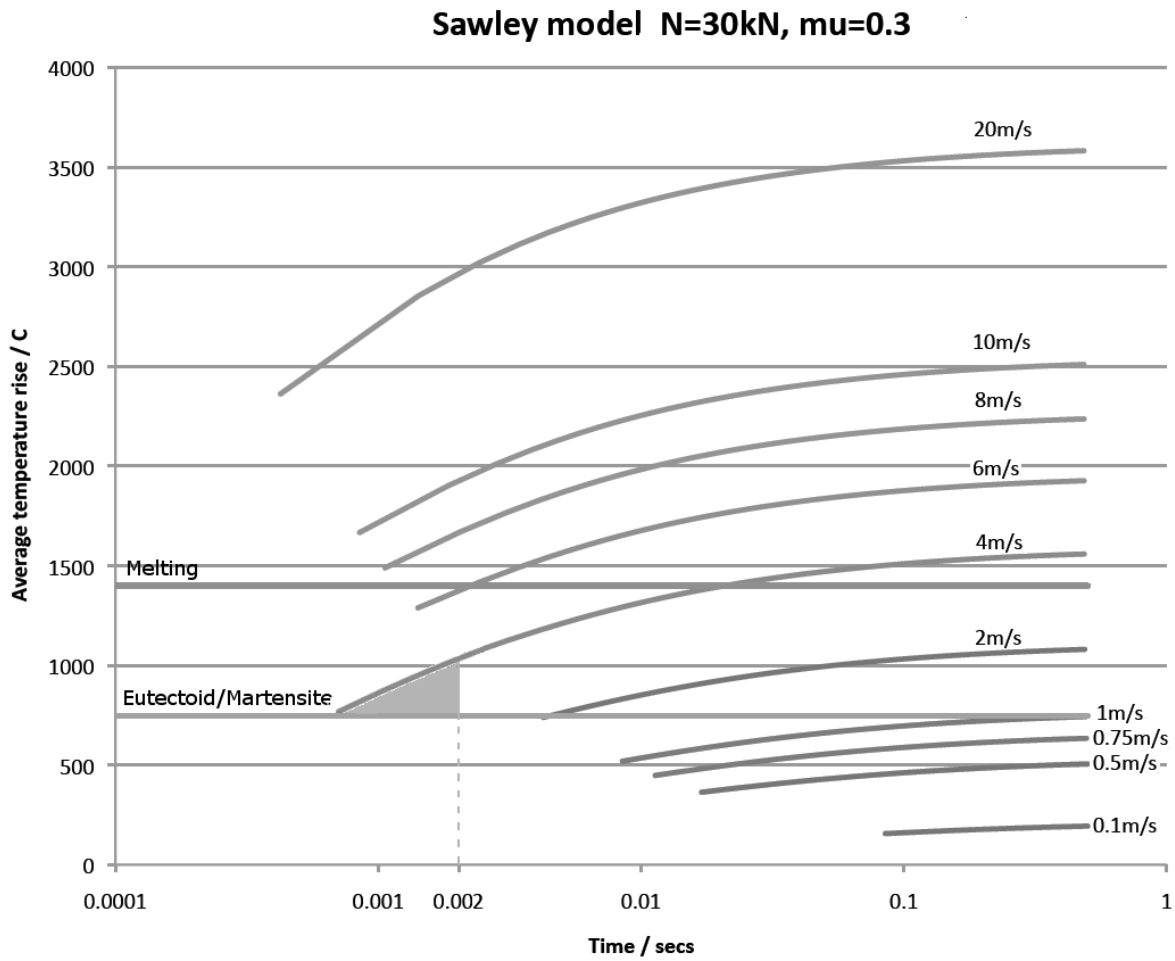

Figure 13 Predicted Temperature Rise versus Duration of Contact for a range of Vehicle Speeds

Considering the longitudinal centre axis of the CP ellipse, the duration of contact for the Figure 12 example is 1.6ms, reducing progressively to zero at the lateral extremities. Therefore, after including a margin for modelling error, the combination of temperature rise with a maximum 2ms thermal duration and a resultant temperature above the eutectoid temperature are the necessary conditions for WEL formation.

Figure 13 shows the Sawley transient thermal model output over a range of vehicle speeds for wheel spin at a friction coefficient of 0.3, which equates to a sudden re-adhesion event as per Figure 12. In practice, at speeds higher than 4m/s (14.4kph) the demanded TE is reducing rapidly (Figure 1) and the likelihood of creep control activity diminishes, in addition to the underlying shortening of contact duration at any single point on the rail. Therefore, the risk of defect generation reduces significantly and quickly above 4m/s for LU rolling stock and track characteristics. However, the thermal model results demonstrate a transient temperature rise above the eutectoid temperature is possible for a narrow range of vehicle speeds, around 3 to 4m/s, which is capable of forming martensite during re-adhesion events. This is highlighted in Figure 13 by the grey shaded area and demonstrates that sufficient thermal energy is present for squat type defects [1] to be initiated.

5. CONCLUSIONS

By simulation methodology it has proved possible to amalgamate electrical, power electronic, control, mechanical and rolling contact disciplines within a single entity. The traction model has demonstrated that a modern wheel-spin control system typically operates in a creep limiting control mode, without reference to the location of the adhesion peak. By evaluation of rail forces resulting from creep control action, assuming typical creep parameters and commonly occurring regions of slightly degraded rail adhesion, it proved possible to identify re-adhesion operating scenarios where high frictional rail surface energy is likely. The requirement for this condition is a modern train, with creep limiting control under maximum acceleration, encountering a sudden change in rail state from damp / lightly contaminated to good / dry conditions.

Separate thermal modelling predicting the transient temperature rise within the contact patch showed that if this re-adhesion scenario occurs at vehicle speeds of 3 - 4m/s (approximately 10 - 15kph) then the resulting

transient energy input to the rail at the wheel contact patch is sufficient to raise the rail to the eutectoid temperature of the steel. Rapid cooling of the rail near surface region from this temperature as the contact area advances results in a martensite transformation of the rail surface to form a white etching layer (WEL). Physical evidence gathered from rails removed from service shows that such layers are associated with crack initiation in the rails studied here, and that this happens without the plastic flow and ratchetting strain accumulation usually associated with crack initiation. The mechanism and growth rate of the thermally initiated defects is the subject of a separate study; however, the understanding of the causation and physical processes involved in defect initiation provided the information needed to intelligently address the problem.

Solutions may lie in modification to the track or in modification of vehicle traction performance. Looking at traction performance solution there are two objectives: firstly, to reduce $T\gamma$ forces during the re-adhesion event, and secondly to reduce either the duration or probability of the event. The first measure reduces the possibility that the temperature conditions required for WEL production are met, while the second restricts the time at risk. The re-adhesion event can only occur during traction creep control; therefore, traction schemes that reduce or avoid extended creep operation will not manifest the problem. However, reversion to old-style DC series motor wheel-spin control would result in performance degradation and longer journey times under moderate or poor rail conditions. Reduction of TE over the critical vehicle speed range is another option, but similarly this affects performance. Such retrospective modifications are difficult to implement and result in timetable impact.

This leaves the option of creep speed limit reduction to restrict $T\gamma$ and the frictional energy during re-adhesion. This still has side effects, increasing the incidence of wheel-spin control activity and demanding superior accuracy of speed measurement, but is considered more acceptable than other options. Work continues to prove the efficacy of this solution, but regardless of the outcome, the capability and potential of multi-speciality simulation has provided a robust understanding of the mechanisms causing thermal 'squat type' rail defects.

6. ACKNOWLEDGMENT

The authors would like to thank London Underground for funding and facilitating this study.

7. REFERENCES

1. **Grassie SL**. Squats and squat-type defects in rails: the understanding to date. Proc IMechE Part F: Journal of Rail and Rapid Transit; doi: 10.1177/0954409711422189, 2011.
2. **Armstrong DS**. Adhesion/Slip Characteristics in Traction. BR Research Technical Memorandum TMTBC015; Dec 1988.
3. **Logston CF Jr** and **Itami GS**. Locomotive Friction - Creep Studies. ASME Paper No. 80-RT-1; 1980.
4. **Fiehn H Weinhardt M and Zeevenhooven N**. Dutch Railways Three Phase Electric Traction Test Vehicle - Adhesion Measurements. Electrische Bahnen; 1979 77 (12); pp. 329-338.
5. **Quarles TL**. Analysis of Performance and Convergence Issues for Circuit Simulation. Spice3 Manual; University of California Berkeley; Memo No. UCB/ERL M89/42; April 1989.
6. **Lewis R and Olofsson U** (eds). Wheel-rail Interface Handbook, section 3 - Wheel-rail contact mechanics. Sep. 2009.
7. **Grassie, SL, Fletcher DI, Hernandez EAG** and **Summers P**. Studs: a squat-type defect in rails; Proc IMechE Part F: Journal of Rail and Rapid Transit; 2011; doi: 10.1177/0954409711421462.
8. **Takahashi J, Kawakami, K** and **Ueda M**. Atom probe tomography analysis of the white etching layer in a rail track surface. 2010; Acta Materialia 58 (2010); pp. 3602–3612.
9. **Osterle W, Rooch H, Pyzalla A** and **Wang L**. Investigation of white etching layers on rails by optical microscopy, electron microscopy, X-ray and synchrotron X-ray diffraction. Materials Science and Engineering A303 (2001); pp. 150 – 157.
10. **Franklin FJ, Garnham JE, Fletcher DI, Davis CL** and **Kapoor A**. Modelling rail steel microstructure and its effect on wear and crack initiation in the UK. WEAR 2008; 265(9-10); pp. 1332-1341.
11. **Fletcher DI**. Thermal contact stress and near surface rail cracks, to be presented at the 9th Int. Conf. on Contact Mechanics and Wear of Rail/Wheel Systems (CM2012). Southwest Jiaotong University, Chengdu, China; 27th-30th August 2012.
12. **Jenkins HH, Stephenson JE, Clayton GA, Morland GW** and **Lyon D**. The effect of track and vehicle parameters on wheel/rail vertical dynamic forces. Proc IMechE, REJ; Jan 1974.
13. **Polach O**. A fast wheel-rail forces calculation computer code. Vehicle System Dynamics; 1999; suppl. 33.
14. **Kalker JJ**. A fast algorithm for the simplified theory of rolling contact. Vehicle System Dynamics; 1982; vol. 11.
15. **Polach O**. Creep forces in simulations of traction vehicles running on adhesion limit. WEAR 258 (2005); pp. 992–1000.
16. **Zaazaa KE** and **Schwab AL**. Review of Joost Kalker's wheel-rail contact theories and their implementation in multibody codes. Proc ASME 2009; Int. Design Engineering DETC2009-87655.
17. **Callister WD**. Phase transformations in metals. Materials Science and Engineering: An Introduction, 2007, ch. 10, 7th edition (John Wiley & Sons); pp. 311–357.

18. **Carslaw HS** and **Jaeger JC**. Conduction of Heat in Solids. Oxford University Press (second edition); 1959.
19. **Ertz M** and **Knothe K**. A comparison of analytical and numerical methods for the calculation of temperatures in wheel/rail contact. WEAR, 2002; vol. 253.
20. **Sawley KJ**. Calculation of temperatures in a sliding wheel/rail system and implications for wheel steel development. Proc IMechE Part F: Journal of Rail and Rapid Transit; July 2007; vol. 221 no. 4.
21. **Fischer FD** and **Schleinzer G**. Residual stress formation and distortion of rail steel. In: Totten G, Howes M and Inoue T (eds) Handbook of Residual Stress and Deformation of Steel, 2002; ASM International; pp. 424-436.